Materials Science & Engineering A 782 (2020) 139281

Contents lists available at ScienceDirect

Materials Science & Engineering A

journal homepage: http://www.elsevier.com/locate/msea

Effect of grain size on the strain rate sensitivity of CoCrFeNi high-entropy alloy

Yakai Zhao [a,b], Xutao Wang [a], Tangqing Cao [a], Jae-Kyung Han [c], Megumi Kawasaki [c], Jae-il Jang [d], Heung Nam Han [e], Upadrasta Ramamurty [b], Lu Wang [a], Yunfei Xue [a,*]

[a] School of Materials Science and Engineering, Beijing Institute of Technology, Beijing, 100081, China
[b] School of Mechanical and Aerospace Engineering, Nanyang Technological University, 639798, Singapore
[c] School of Mechanical, Industrial & Manufacturing Engineering, Oregon State University, Corvallis, OR, 97331, USA
[d] Division of Materials Science and Engineering, Hanyang University, Seoul, 04763, Republic of Korea
[e] Department of Materials Science and Engineering, Seoul National University, Seoul, 08826, Republic of Korea

ARTICLE INFO

Keywords:
High-entropy alloy
Grain size effect
High-pressure torsion
Nanoindentation
Strain-rate sensitivity

ABSTRACT

Strain rate sensitivity (SRS) of a face-centered cubic (fcc) CoCrFeNi high-entropy alloy (HEA) with grain sizes ranging from 57 μm to 45 nm was investigated using nanoindentation, and was compared with those reported for conventional fcc metals. Experimental results show pronounced grain boundary strengthening in the HEA. Estimated values of the SRS parameter, m and activation volume, V^*, indicate similar plastic deformation mechanisms in HEA and Ni in nanocrystalline regime that are grain boundary mediated. In coarse-grained regime, the high lattice friction stress in the HEA results in much higher m and smaller V^* as compared to coarse grained Ni.

High-entropy alloys (HEAs) significantly widen the principles of alloy design and engineering [1]. Among many different HEAs, the face-centered cubic (fcc) HEAs are most widely studied, due to their interesting attributes such as simple structure, severe lattice distortion, sluggish diffusion, and promising mechanical properties [1–3]. Single phase fcc HEAs usually show low tensile strength at room temperature. Consequently, mechanisms such as the grain boundary (GB) strengthening [4], precipitation strengthening [5], and transformation-induced plasticity (TRIP) [3] are explored so as to improve their strength.

The lattice friction stress in conventional fcc metals and alloys is relatively small, making them readily amenable to dislocation glide. In contrast, fcc HEAs possess higher friction stresses, possibly due to lattice distortions and variations in dislocation velocity [6]. Such high lattice friction may be one of the reasons causing relatively enhanced strain-rate sensitivity (SRS) observed in many fcc HEAs [4]. Recently, it has been reported that high-pressure torsion (HPT) processing can significantly reduce the average grain size, d, of HEAs from several tens of μm to several tens of nm (i.e., the nanocrystalline (nc) regime) and correspondingly the mechanical performance of HPT-processed HEAs can be largely enhanced [4]. A detailed understanding of the coupling between the Hall-Petch strengthening, which is pronounced in HEAs, and the solid solution strengthening is essential for identifying strategies for strengthening of HEAs. Keeping this in view, we examine SRS of a single-phase fcc CoCrFeNi HEA with a wide ranging d. Through a comparison of the results with those of conventional fcc metals and alloys, the dominant deformation mechanisms at different d are identified and discussed.

Vacuum induction melting of pure metals (purity > 99.9 wt%) and drop casting were utilized to synthesize the $Co_{25}Cr_{25}Fe_{25}Ni_{25}$ (in at.%) HEA. The thickness of the cast ingot was reduced by ~64% via hot-rolling at 1050 °C. It was then homogenized for 1 h at 1100 °C (samples denoted as "AH" hereafter). The AH samples were subjected to two processing routes to produce the samples with different d. In the first route, the AH samples were cold rolled to reduce their thickness by ~60% and then annealed for 1 h at either 800 or 1100 °C (denoted as "800A" and "1100A" samples, respectively). In the second route, 10 mm diameter discs with ~0.85 mm thickness were machined from the AH samples. They were subjected to HPT under "quasi-constrained" configuration and an applied pressure of 6.0 GPa for 1/4, 2, and 5 turns (denoted as "HPT1/4," "HPT2," and "HPT5" samples, respectively) at 1 rpm.

Microstructures of the specimens were examined by electron back-

* Corresponding author.
E-mail address: xueyunfei@bit.edu.cn (Y. Xue).

https://doi.org/10.1016/j.msea.2020.139281
Received 28 January 2020; Received in revised form 18 March 2020; Accepted 19 March 2020
Available online 23 March 2020

scattered diffraction (EBSD) (NordlysNano, Oxford Instruments, Abingdon, UK) and TEM (Tecnai G^2 F20, FEI Co., Hillsboro, OR, USA). EBSD measurements (and subsequent mechanical tests) on 800A and 1100A samples were made on the surface perpendicular to the cold rolling direction. All the samples were polished with fine SiC papers and then 0.04 μm colloidal silica suspension to a mirror finish. A thin layer was milled by focused ion beam from the vertical cross-sections at the edges of the HPT-processed discs and lifted for TEM. Nanoindentation experiments were conducted on annealed specimens and at the edge of each HPT-processed specimen using a Nanoindenter-XP (KLA, Milpitas, CA, USA) instrument equipped with a Berkovich tip at a maximum load of 100 mN under indentation strain rates $\dot{\varepsilon}_i$ (= (dh/dt)/h, where h is depth and t is time) of 0.01, 0.025, and 0.1 s^{-1}.

Fig. 1a and b shows the EBSD maps of 1100A and 800A specimens, respectively. No preferred texture was displayed for both samples, and d was determined as ~57 ± 20 μm for 1100A and ~11 ± 8 μm for 800A. HPT generally induces significant gradient in the microstructure and hence mechanical properties within the processed disc [4,7], which is also clear in this study (see Fig. S1 in supplementary material); the HV value increases markedly with the distance from the center, suggesting that microstructural evolution occurs most severely in the peripheral regions of the disc. Therefore, to ensure the reliability and reproducibility of the results, all the microstructure and mechanical properties characterizations of HPT samples were performed near the edge part of each disc. While the selected area electron diffraction (SAED) patterns of the edge regions in the HPT discs (see Fig. 1c–e) reveal a single-phase fcc structure, the bright-field images show substantial grain refinement without the formation of any new phase. From such images, d in HPT1/4, HPT2, and HPT5 samples were estimated to be ~77 ± 31, ~46 ± 16, and ~45 ± 15 nm, respectively. These data clearly show that nc structure forms readily at the disc periphery in the early stage (merely 1/4 turn) of HPT; a further and gradual decrease in d with the number of turns, N, until d saturates after N = 2. In addition to the significant atomic diffusivity enhancement during HPT process [4], relatively low stacking fault energy (SFE) of CoCrFeNi HEA (~32.5 mJ/m^2 [8]) can be a possible reason for the dramatic grain refinement. Low SFE is known to lead to a reduced value d in materials that were subjected to HPT by altering grain refinement mechanism and restricting recovery process [9]. Indeed, it was proposed [10,11] that the HPT-induced grain refinement mechanism in the CoCrFeNi HEA includes concurrent

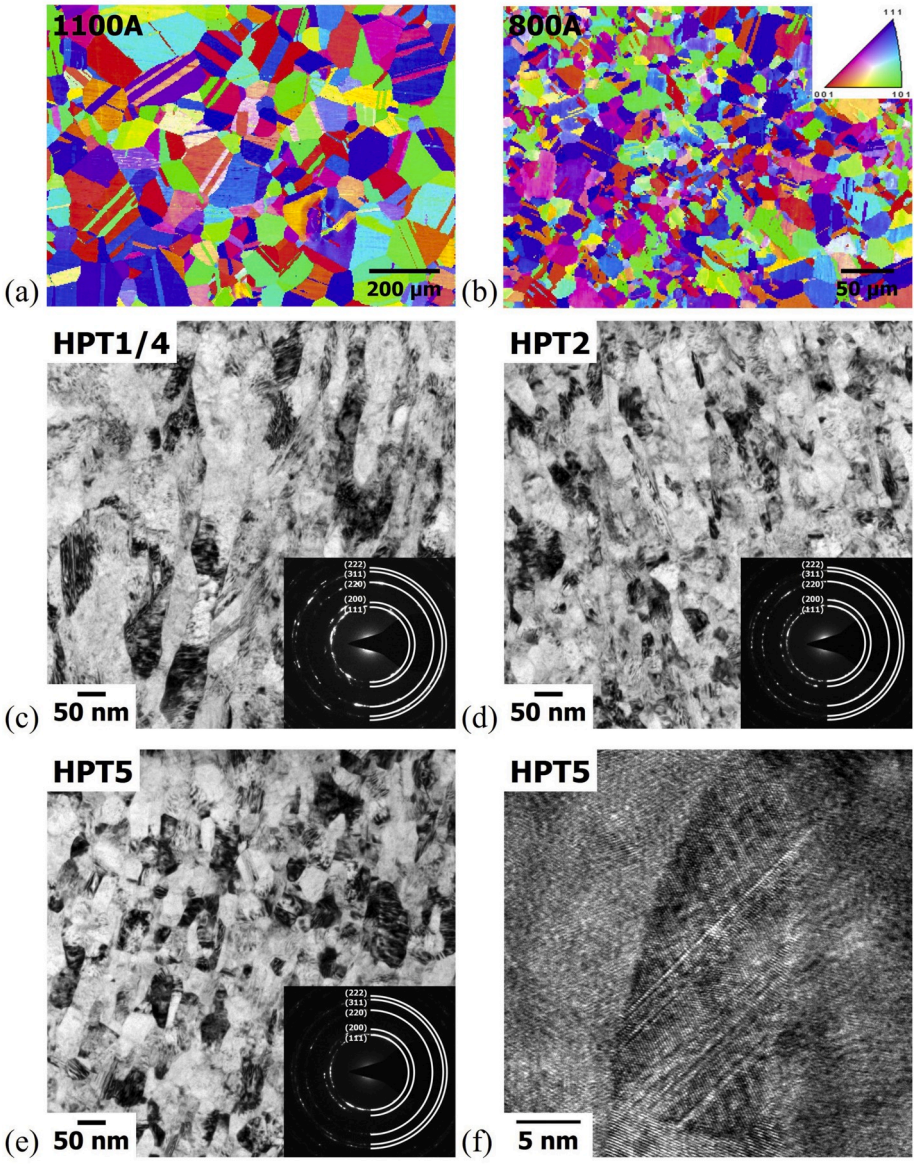

Fig. 1. Microstructure of CoCrFeNi HEA samples, including EBSD maps of (a) 1100A and (b) 800A, TEM images accompanied with SAED patterns of (c) HPT1/4, (d) HPT2, and (e) HPT5, and (f) the HRTEM image of a typical nano-grain in HPT5 sample containing stacking faults and nanoscale twins.

nanoband subdivision and deformation twinning which are different from the conventional mechanisms. Such a scenario agrees with our high-resolution TEM (HRTEM) observations showing high density of stacking faults and nanotwins, which are only a few atomic layer thick, within the nc grains of HPT5 sample (Fig. 1f).

Representative nanoindentation load–displacement (*P–h*) responses measured at $\dot{\varepsilon}_i = 0.025\ s^{-1}$ are displayed in Fig. 2. It can be seen that (1) the HPT-processed samples show much smaller maximum displacement, h_{max}, at the peak load, as compared to h_{max} in 1100A and 800A samples, and (2) the h_{max} values for the HPT-processed discs become smaller with increasing *N*. The trends at different $\dot{\varepsilon}_i$ were similar (and hence not shown). The inset of Fig. 2 displays *P–h* responses obtained on 1100A and HPT1 samples. A perceptible shift in the responses (indicated by the arrows) with increasing $\dot{\varepsilon}_i$ is noted; h_{max} decreases with increasing $\dot{\varepsilon}_i$ for both annealed and HPT-processed HEA samples, suggesting a positive strain-rate dependence of plastic flow.

Fig. 3 summarizes the variations in nanoindentation hardness *H* as a function of $d^{-1/2}$, as in the Hall-Petch (HP) relationship, $H = H_0 + k_{HP}d^{-1/2}$ (where H_0 is the material's intrinsic hardness and k_{HP} is the locking parameter [4,12]), at three different $\dot{\varepsilon}_i$. In all the three cases, an increase in *H* with decreasing *d* is seen, i.e., no "inverse HP effect" was seen. This is probably due to the fact that the transition from classical to inverse HP relation was observed to occur only when *d* is less than ~10–20 nm [13]). Since the smallest *d* of the current study (~45 nm) is significantly larger than those critical *d* values, it is not surprising that *H* vs. *d* plots obey the classical HP relation. As expected from the *P–h* curves in Fig. 2, the estimated *H* for the specimens is evidently rate-sensitive and increases with $\dot{\varepsilon}_i$. It is also apparent in Fig. 3 that when *d* is reduced from ~57 μm down to ~45 nm, average *H* values become more than triple, for example, from ~2.14 to ~6.91 GPa at $\dot{\varepsilon}_i$ of 0.025 s^{-1}. Possible reasons for such significant grain-size strengthening could be the marked reduction in *d* due to HPT process and a high k_{HP}. Values of H_0 and k_{HP}, estimated through the best fits of the HP relationship to data in Fig. 3, are listed in Table 1. The data suggest that both H_0 and k_{HP} show very weak strain-rate dependence (only marginally increase by ~6% and ~4%, respectively). More importantly, the values of k_{HP} (~1018–1056 MPa $\mu m^{1/2}$) for the CoCrFeNi HEA are much higher than those reported for conventional fcc metals (≤600 MPa $\mu m^{1/2}$ [14]).

To quantitatively estimate the GB strengthening capability in the HEA, the critical resolved shear stress required to operate plastic flow across GB, τ_c, can be estimated on the basis of the dislocation pile-up model as [15]:

$$k_{HP} = 3M(\pi m_s \tau_c G b/2\alpha)^{1/2} \quad (1)$$

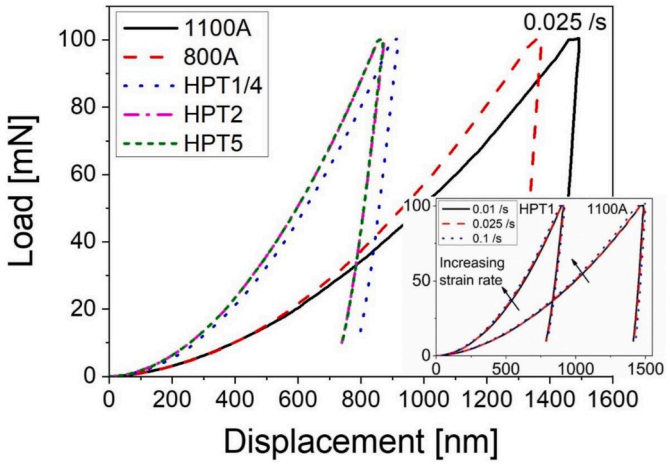

Fig. 2. Representative load-displacement curves of all the samples obtained at a fixed $\dot{\varepsilon}_i$ of 0.025 s^{-1} (with inset showing the curves of 1100A and HPT1 samples obtained at different $\dot{\varepsilon}_i$).

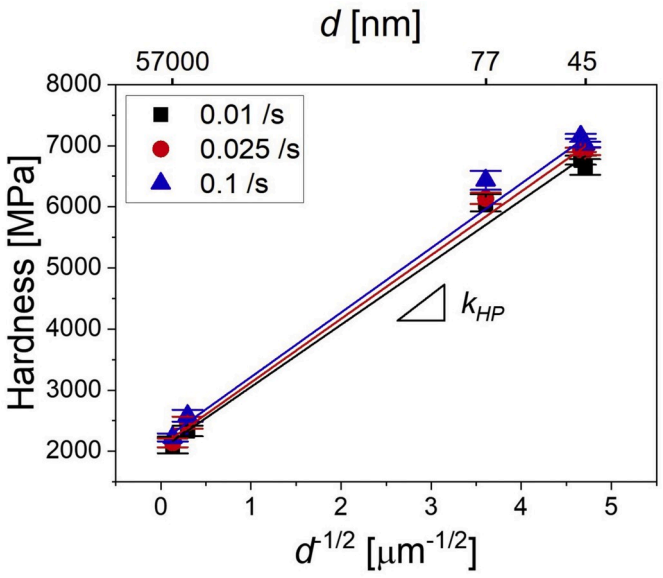

Fig. 3. Changes in hardness as a function of $d^{-1/2}$ under different $\dot{\varepsilon}_i$.

Table 1
The average values of H_0, k_{HP}, and τ_c at different $\dot{\varepsilon}_i$.

$\dot{\varepsilon}_i$ [s^{-1}]	H_0 [GPa]	k_{HP} [MPa·$\mu m^{1/2}$]	τ_c [MPa]
0.01	2.034 ± 0.130	1018 ± 37	138
0.025	2.083 ± 0.129	1042 ± 31	145
0.1	2.158 ± 0.152	1056 ± 37	149

where the ratio of 3 is from the well-accepted Tabor's relation between indentation hardness and yield strength of a material, *M* is the Taylor factor (taken as 3.06 for fcc), m_s is Sachs orientation factor (2.238 [12]), *G* is shear modulus (~82 GPa [6]), *b* is the magnitude of Burgers vector (calculated as $b = a_0 \times \sqrt{2}/2 \approx 2.25 \times 10^{-10}$ m where a_0 is the lattice parameter for CoCrFeNi, ~0.357 nm [16]), α is average dislocation character obtained by $\alpha = 2(1\text{-}\nu)/(2\text{-}\nu)$ (ν is Poisson's ratio, taken as 0.28 [16]). The τ_c values calculated from Eq. (1) are listed in Table 1. Similar to k_{HP}, τ_c does not vary significantly with different $\dot{\varepsilon}_i$. Importantly, τ_c of CoCrFeNi HEA (~138–149 MPa) are much higher than those reported for pure fcc metals (e.g. 21.9 MPa for Cu and 36.7 MPa for Ni [14]), and suggest, as with k_{HP}, more effective GB strengthening in fcc HEAs than in conventional fcc metals. Interestingly, these τ_c values are still smaller than those of bcc metals (e.g. 221 MPa for Cr and 420 MPa for Ta [14]), implying that GB strengthening ability in fcc HEA may range between those of conventional fcc and bcc metals.

From the relation between *H* and $\dot{\varepsilon}_i$ in Fig. 3, we estimated the SRS parameter, $m = \frac{\partial \ln(H/C)}{\partial \ln \dot{\varepsilon}_i}$ (where *C* is constraint factor [4]), and the activation volume, $V^* = \sqrt{3}kT\frac{\partial \ln \dot{\varepsilon}_i}{\partial (H/C)}$ (where *k* is Boltzmann's constant and *T* is absolute temperature), as shown in Fig. S2 in supplementary material. Estimated values of *m* and *V** provide insights into the predominant plastic deformation mechanism. It was shown earlier that the value of *V** varies by orders of magnitude for different rate-limiting processes with typical values of ~$100b^3$ to ~$1000b^3$ for dislocation forest cutting in coarse-grained (cg) fcc metals, ~$10b^3$ for GB sliding, and ~$1b^3$ to ~$10b^3$ for diffusion either along GBs or through the crystalline lattice [17,18].

To better understand the differences in the deformation mechanisms of fcc HEAs and conventional fcc metals and alloys, the results of *m* and *V** for the current CoCrFeNi samples are plotted as a function of *d* along with those of fcc HEAs from literature [4,16,19–26] [27] in Fig. 4a and c. The literature data for pure Ni [17,28–33] and binary Ni alloys [33–35] are presented in Fig. 4b and d for comparison. For clarity, all the data in

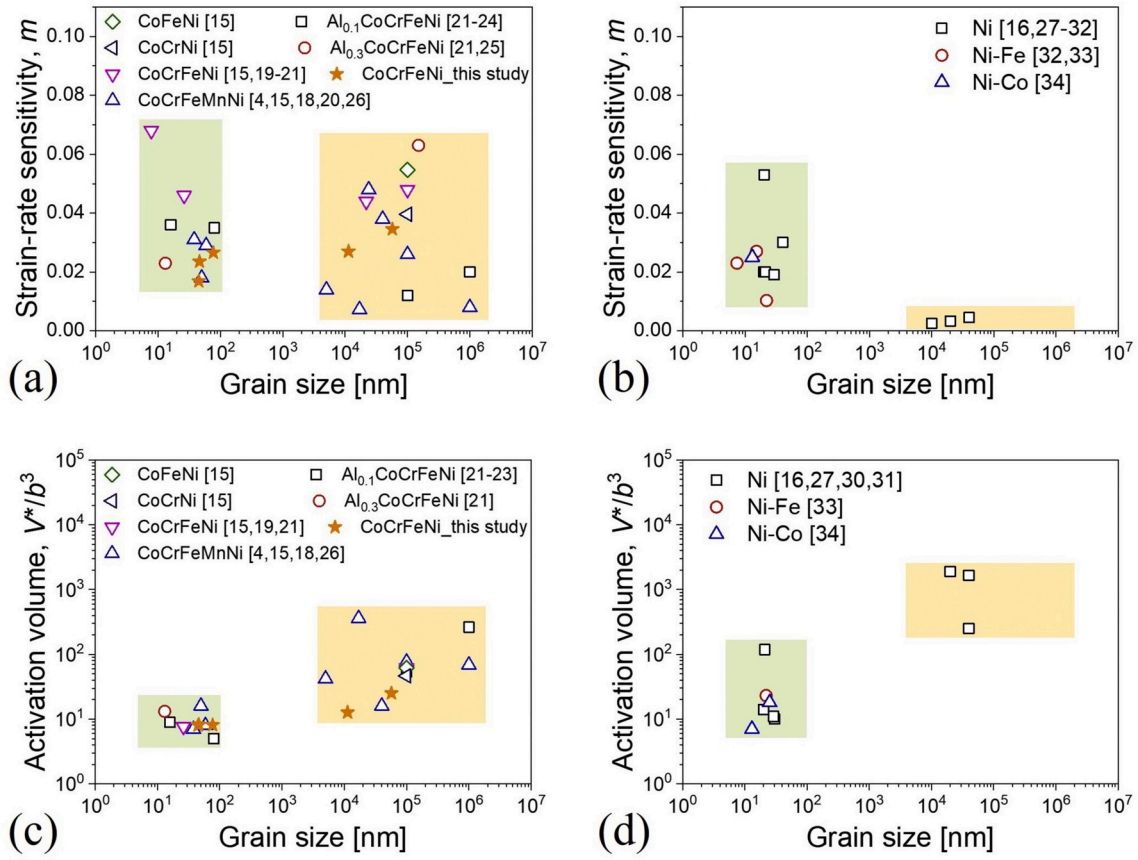

Fig. 4. (a) and (b) Strain-rate sensitivity and (c) and (d) activation volume values of fcc HEAs and pure Ni from literature. (a) and (c) are for fcc HEAs [4,16,19–27], and (b) and (d) are for pure Ni and binary Ni alloys [17,28–35].

Fig. 4 are categorized into two separate range of d, i.e. ~5–100 nm (nc range) and ~4–200 μm (cg range). In Fig. 4, in the nc regime the m values for fcc HEAs of ~0.016–0.07 and pure Ni of ~0.010–0.055 are in the similar range, whereas in the cg regime, the m values show a significant discrepancy (~0.007–0.06 for HEAs vs. ~0.002–0.005 for Ni). Similar trends are also noted for V^* values. The good agreement between the m values of the nc HEAs and nc Ni (and nc binary Ni alloys) suggests that the deformation mechanisms in them are similar. In contrast, the difference in the deformation mechanisms between the cg HEAs and cg Ni is responsible for the lack of a clear trend in the relation of m vs. d in HEAs.

In conventional fcc metals and alloys, m unambiguously increases with reducing d to the nc regime, as in Fig. 4b, and V^* for dislocation-mediated flow decreases through grain refinement since GBs begin to play an important role in the plastic flow by both interacting with dislocations and introducing dislocations [17]. Since the V^* values for the nc HEAs are also around ~$10b^3$, it appears that the deformation mechanism is consistent with the conventional nc metals, i.e. GB-mediated dislocation activity (dislocation nucleation and/or dislocation depinning at GBs [17,28]).

The relatively higher m in cg HEAs can be understood by considering the characteristics in their atomic-level structure. In conventional cg fcc metals, the rate-limiting deformation mechanism is dislocation forest cutting, corresponding to V^* values in the range of ~100–1000b^3 [17]. In Fig. 4c, fcc HEAs show much less V^* values (mostly at the magnitude of ~$10b^3$), suggesting that the short-range barriers, which are responsible for thermal-activated deformation [18,25], are enhanced. This is because HEAs possess high lattice friction stress, resulting in much stronger Peierls barrier to dislocation motion than conventional fcc metals [16,36]. In addition, it has been proved that chemical short-range ordering occurs in the atomic structure of HEAs [37]. Such ordering is also responsible for the high friction stress in the HEAs and thus contributes to the thermal activated process, or more specifically, reducing the V^* in the cg HEAs [16,23,36].

In summary, the influence of varying grain size on the rate-sensitive nanomechanical behavior of CoCrFeNi HEA was investigated through nanoindentation. The results suggest that the hardness of the HEA can be increased by more than 300% through grain size refinement to nc regime via HPT. This hardness enhancement was attributed to a much higher Hall-Petch coefficient for the fcc HEAs than conventional fcc metals, which originates from the enhanced values of τ_c in the former. Through the estimated values of the rate-sensitive parameters, m and V^*, of the HEA with different grain sizes and comparing them with those of conventional fcc alloys, we show that the mechanisms for the nc HEA and the nc Ni are similar; in nc regime, plastic deformation in both of them is governed by GB-mediated process. The predominant deformation mechanisms for the cg HEA and the cg Ni are significantly different; the cg HEA possesses high friction stress, resulting in much higher m and smaller V^* than the cg Ni.

Data availability

The data that support the findings of this study are available from the corresponding author on reasonable request.

Declaration of competing interest

The authors declare that they have no known competing financial interests or personal relationships that could have appeared to influence the work reported in this paper.

CRediT authorship contribution statement

Yakai Zhao: Conceptualization, Formal analysis, Investigation, Data curation, Visualization, Writing - original draft. **Xutao Wang:** Resources, Formal analysis. **Tangqing Cao:** Resources, Formal analysis. **Jae-Kyung Han:** Resources, Formal analysis. **Megumi Kawasaki:** Resources, Formal analysis, Writing - review & editing. **Jae-il Jang:** Methodology, Writing - review & editing. **Heung Nam Han:** Writing - review & editing. **Upadrasta Ramamurty:** Supervision, Writing - review & editing. **Lu Wang:** Project administration, Supervision. **Yunfei Xue:** Supervision, Writing - review & editing, Funding acquisition.

Acknowledgements

The work at BIT was supported by the National Key Research and Development Program of China (grant number 2018YFB0703403). The work at Hanyang University was supported by the National Research Foundation of Korea (NRF) grants funded by the Korea government (MSIT) (No. 2020R1A2B5B01001446 and No. 2020R1A5A6017701) The work at Oregon State University was supported by the National Science Foundation of the United States (Grant No. DMR-1810343).

Appendix A. Supplementary data

Supplementary data to this article can be found online at https://doi.org/10.1016/j.msea.2020.139281.

References

[1] D.B. Miracle, O.N. Senkov, A critical review of high entropy alloys and related concepts, Acta Mater. 122 (2017) 448–511, https://doi.org/10.1016/j.actamat.2016.08.081.
[2] Y. Zhao, D.H. Lee, M.Y. Seok, J.A. Lee, M.P. Phaniraj, J.Y. Suh, H.Y. Ha, J.Y. Kim, U. Ramamurty, J. il Jang, Resistance of CoCrFeMnNi high-entropy alloy to gaseous hydrogen embrittlement, Scripta Mater. 135 (2017) 54–58, https://doi.org/10.1016/j.scriptamat.2017.03.029.
[3] Z. Li, K.G. Pradeep, Y. Deng, D. Raabe, C.C. Tasan, Metastable high-entropy dual-phase alloys overcome the strength-ductility trade-off, Nature 534 (2016) 227–230, https://doi.org/10.1038/nature17981.
[4] D.-H. Lee, I.-C. Choi, M.-Y. Seok, J. He, Z. Lu, J.-Y. Suh, M. Kawasaki, T. G. Langdon, J. Jang, Nanomechanical behavior and structural stability of a nanocrystalline CoCrFeNiMn high-entropy alloy processed by high-pressure torsion, J. Mater. Res. 30 (2015) 2804–2815, https://doi.org/10.1557/jmr.2015.239.
[5] J.Y. He, H. Wang, H.L. Huang, X.D. Xu, M.W. Chen, Y. Wu, X.J. Liu, T.G. Nieh, K. An, Z.P. Lu, A precipitation-hardened high-entropy alloy with outstanding tensile properties, Acta Mater. 102 (2016) 187–196, https://doi.org/10.1016/j.actamat.2015.08.076.
[6] Z. Wu, H. Bei, G.M. Pharr, E.P. George, Temperature dependence of the mechanical properties of equiatomic solid solution alloys with face-centered cubic crystal structures, Acta Mater. 81 (2014) 428–441, https://doi.org/10.1016/j.actamat.2014.08.026.
[7] A.P. Zhilyaev, T.G. Langdon, Using high-pressure torsion for metal processing: fundamentals and applications, Prog. Mater. Sci. 53 (2008) 893–979, https://doi.org/10.1016/j.pmatsci.2008.03.002.
[8] Y. Wang, B. Liu, K. Yan, M. Wang, S. Kabra, Y.L. Chiu, D. Dye, P.D. Lee, Y. Liu, B. Cai, Probing deformation mechanisms of a FeCoCrNi high-entropy alloy at 293 and 77 K using in situ neutron diffraction, Acta Mater. 154 (2018) 79–89, https://doi.org/10.1016/j.actamat.2018.05.013.
[9] Y.H. Zhao, X.Z. Liao, Y.T. Zhu, Z. Horita, T.G. Langdon, Influence of stacking fault energy on nanostructure formation under high pressure torsion, Mater. Sci. Eng. A (2005) 188–193, https://doi.org/10.1016/j.msea.2005.08.074, 410–411.
[10] J. Gubicza, P.T. Hung, M. Kawasaki, J. Han, Y. Zhao, Y. Xue, J.L. Lábár, Influence of severe plastic deformation on the microstructure and hardness of a CoCrFeNi high-entropy alloy: a comparison with CoCrFeNiMn, Mater. Char. 154 (2019) 304–314, https://doi.org/10.1016/j.matchar.2019.06.015.
[11] W. Wu, M. Song, S. Ni, J. Wang, Y. Liu, B. Liu, X. Liao, Dual mechanisms of grain refinement in a FeCoCrNi high- entropy alloy processed by high- pressure torsion, Sci. Rep. 7 (2017) 46720, https://doi.org/10.1038/srep46720.
[12] R.W. Cahn, P. Haasen, Physical Metallurgy, fourth ed., Cambridge University Press, Amsterdam, 1996. https://www.sciencedirect.com/book/9780444898753/physical-metallurgy.
[13] C.S. Pande, K.P. Cooper, Nanomechanics of Hall-Petch relationship in nanocrystalline materials, Prog. Mater. Sci. 54 (2009) 689–706, https://doi.org/10.1016/j.pmatsci.2009.03.008.
[14] D. Wu, J. Zhang, J.C. Huang, H. Bei, T.G. Nieh, Grain-boundary strengthening in nanocrystalline chromium and the Hall-Petch coefficient of body-centered cubic metals, Scripta Mater. 68 (2013) 118–121, https://doi.org/10.1016/j.scriptamat.2012.09.025.
[15] R.W. Armstrong, P. Rodriguez, Flow stress/strain rate/grain size coupling for fcc nanopolycrystals, Philos. Mag. 86 (2006) 5787–5796, https://doi.org/10.1080/14786430600764872.
[16] Z. Wu, Y. Gao, H. Bei, Thermal activation mechanisms and Labusch-type strengthening analysis for a family of high-entropy and equiatomic solid-solution alloys, Acta Mater. 120 (2016) 108–119, https://doi.org/10.1016/j.actamat.2016.08.047.
[17] Y.M. Wang, A.V. Hamza, E. Ma, Temperature-dependent strain rate sensitivity and activation volume of nanocrystalline Ni, Acta Mater. 54 (2006) 2715–2726, https://doi.org/10.1016/j.actamat.2006.02.013.
[18] D. Caillard, J.L. Martin, Thermally Activated Mechanisms in Crystal Plasticity, Pergamon, Amsterdam, 2003.
[19] V. Maier-Kiener, B. Schuh, E.P. George, H. Clemens, A. Hohenwarter, Insights into the deformation behavior of the CrMnFeCoNi high-entropy alloy revealed by elevated temperature nanoindentation, J. Mater. Res. 32 (2017) 2658–2667, https://doi.org/10.1557/jmr.2017.260.
[20] W. Huo, F. Fang, X. Liu, S. Tan, Z. Xie, J. Jiang, Remarkable strain-rate sensitivity of nanotwinned CoCrFeNi alloys, Appl. Phys. Lett. 114 (2019) 101904, https://doi.org/10.1063/1.5088921.
[21] M. Shabani, J. Indeck, K. Hazeli, P.D. Jablonski, G.J. Pataky, Effect of strain rate on the tensile behavior of CoCrFeNi and CoCrFeMnNi high-entropy alloys, J. Mater. Eng. Perform. 28 (2019) 4348–4356, https://doi.org/10.1007/s11665-019-04176-y.
[22] X.B. Feng, W. Fu, J.Y. Zhang, J.T. Zhao, J. Li, K. Wu, G. Liu, J. Sun, Effects of nanotwins on the mechanical properties of AlxCoCrFeNi high entropy alloy thin films, Scripta Mater. 139 (2017) 71–76, https://doi.org/10.1016/j.scriptamat.2017.06.009.
[23] M. Komarasamy, N. Kumar, R.S. Mishra, P.K. Liaw, Anomalies in the deformation mechanism and kinetics of coarse-grained high entropy alloy, Mater. Sci. Eng. A 654 (2016) 256–263, https://doi.org/10.1016/j.msea.2015.12.063.
[24] P.F. Yu, H. Cheng, L.J. Zhang, H. Zhang, Q. Jing, M.Z. Ma, P.K. Liaw, G. Li, R.P. Liu, Effects of high pressure torsion on microstructures and properties of an Al0.1CoCrFeNi high-entropy alloy, Mater. Sci. Eng. A 655 (2016) 283–291, https://doi.org/10.1016/j.msea.2015.12.085.
[25] S. Gangireddy, B. Gwalani, R.S. Mishra, Grain size dependence of strain rate sensitivity in a single phase FCC high entropy alloy Al0.3CoCrFeNi, Mater. Sci. Eng. A 736 (2018) 344–348, https://doi.org/10.1016/j.msea.2018.09.009.
[26] S. Gangireddy, B. Gwalani, V. Soni, R. Banerjee, R.S. Mishra, Contrasting mechanical behavior in precipitation hardenable Al X CoCrFeNi high entropy alloy microstructures: single phase FCC vs. dual phase FCC-BCC, Mater. Sci. Eng. A 739 (2019) 158–166, https://doi.org/10.1016/j.msea.2018.10.021.
[27] G. Laplanche, J. Bonneville, C. Varvenne, W.A. Curtin, E.P. George, Thermal activation parameters of plastic flow reveal deformation mechanisms in the CrMnFeCoNi high-entropy alloy, Acta Mater. 143 (2018) 257–264, https://doi.org/10.1016/j.actamat.2017.10.014.
[28] C.D. Gu, J.S. Lian, Q. Jiang, W.T. Zheng, Experimental and modelling investigations on strain rate sensitivity of an electrodeposited 20 nm grain sized Ni, J. Phys. D Appl. Phys. 40 (2007) 7440–7446, https://doi.org/10.1088/0022-3727/40/23/027.
[29] F. Dalla Torre, H. Van Swygenhoven, M. Victoria, Nanocrystalline electrodeposited Ni: microstructure and tensile properties, Acta Mater. 50 (2002) 3957–3970, https://doi.org/10.1016/S1359-6454(02)00198-2.
[30] R. Schwaiger, B. Moser, M. Dao, N. Chollacoop, S. Suresh, Some critical experiments on the strain-rate sensitivity of nanocrystalline nickel, Acta Mater. 51 (2003) 5159–5172, https://doi.org/10.1016/S1359-6454(03)00365-3.
[31] Y.M. Wang, A.V. Hamza, E. Ma, Activation volume and density of mobile dislocations in plastically deforming nanocrystalline Ni, Appl. Phys. Lett. 86 (2005) 241917, https://doi.org/10.1063/1.1946899.
[32] F.D. Torre, P. Spätig, R. Schäublin, M. Victoria, Deformation behaviour and microstructure of nanocrystalline electrodeposited and high pressure torsioned nickel, Acta Mater. 53 (2005) 2337–2349, https://doi.org/10.1016/j.actamat.2005.01.041.
[33] T. Guo, P. Huang, K.W. Xu, F. Wang, T.J. Lu, Solid solution effects on hardness and strain rate sensitivity of nanocrystalline NiFe alloy, Mater. Sci. Eng. A 676 (2016) 501–505, https://doi.org/10.1016/j.msea.2016.08.120.
[34] H. Li, H. Choo, P.K. Liaw, The effect of temperature on strain rate sensitivity in a nanocrystalline Ni–Fe alloy, J. Appl. Phys. 101 (2007), 063536, https://doi.org/10.1063/1.2711411.
[35] C. Gu, J. Lian, Q. Jiang, Z. Jiang, Ductile-brittle-ductile transition in an electrodeposited 13 nanometer grain sized Ni-8.6 wt.% Co alloy, Mater. Sci. Eng. A 459 (2007) 75–81, https://doi.org/10.1016/j.msea.2006.12.093.
[36] J. Moon, S.I. Hong, J.B. Seol, J.W. Bae, J.M. Park, H.S. Kim, Strain-rate sensitivity of high-entropy alloys and its significance in deformation, Mater. Res. Lett. 7 (2019) 503–509, https://doi.org/10.1080/21663831.2019.1668489.
[37] C. Niu, A.J. Zaddach, A.A. Oni, X. Sang, J.W. Hurt, J.M. LeBeau, C.C. Koch, D. L. Irving, Spin-driven ordering of Cr in the equiatomic high entropy alloy NiFeCrCo, Appl. Phys. Lett. 106 (2015) 161906, https://doi.org/10.1063/1.4918996.